HHS Public Access

Author manuscript

Oncogene. Author manuscript; available in PMC 2022 May 12.

Published in final edited form as:

Oncogene. 2022 January ; 41(3): 414–426. doi:10.1038/s41388-021-02110-y.

MZF1 mediates oncogene-induced senescence by promoting the transcription of p16^{INK4A}

Dan Wu[1,#], **Hua Tan**[2,#], **Weijun Su**[3], **Dongmei Cheng**[1], **Guanwen Wang**[1,3], **Juan Wang**[1,3], **Ding A. Ma**[1], **George M. Dong**[1], **Peiqing Sun**[1,*]

[1]Departments of Cancer Biology, Comprehensive Cancer Center, Wake Forest Baptist Medical Center, Medical Center Blvd, Winston-Salem, NC 27157, USA

[2]School of Biomedical Informatics, University of Texas Health Science Center at Houston, Houston, TX, 77030, USA

[3]Nankai University School of Medicine, Tianjin, China

Abstract

Oncogene induced senescence is a tumor suppressing defense mechanism, in which the cell cycle-dependent protein kinase (CDK) inhibitor p16^{INK4A} (encoded by the CDKN2A gene) plays a key role. We previously reported that a transcriptional co-activator chromodomain helicase DNA binding protein 7 (CHD7) mediates oncogenic *ras*-induced senescence by inducing transcription of the p16^{INK4A} gene. In the current study, we identified myeloid zinc finger 1 (MZF1) as the transcriptional factor that recruits CHD7 to the p16^{INK4A} promoter, where it mediates oncogenic *ras*-induced p16^{INK4A} transcription and senescence through CHD7, in primary human cells from multiple origins. Moreover, the expression of MZF1 is induced by oncogenic *ras* in senescent cells through the c-Jun and Ets1 transcriptional factors upon their activation by the Ras-Raf-1-MEK-ERK signaling pathway. In non-small cell lung cancer (NSCLC) and pancreatic adenocarcinoma (PAAD) where activating *ras* mutations occur frequently, reduced MZF1 expression is observed in tumors, as compared to corresponding normal tissues, and correlates with poor patient survival. Analysis of single cell RNA-sequencing data from PAAD patients revealed that among the tumor cells with normal RB expression levels, those with reduced levels of MZF1 are more likely to express lower p16^{INK4A} levels. These findings have identified novel signaling components in the pathway that mediates induction of the p16^{INK4A} tumor suppressor and the senescence response, and suggested that MZF1 is a potential tumor suppressor in at least some cancer types, the loss of which contributes to inactivation of the p16^{INK4A}/RB pathway and disruption of senescence in tumor cells with intact RB.

[*]Corresponding author: Peiqing Sun, Department of Cancer Biology, Wake Forest Baptist Comprehensive Cancer Center, Wake Forest Baptist Medical Center, Medical Center Blvd, Winston-Salem, NC 27157. 336-716-5066 (Tel), 336-716-0255 (Fax), psun@wakehealth.edu.

[#]These authors contribute equally to the work.

Author contributions

DW, HT, WS and PS conceived and designed the study. DW, HT, WS, DC, GW, JW, DAM and GMD executed the experiments; DW, HT, WS, DAM, GMW and PS analyzed and interpreted the data. DW, HT and PS wrote and/or reviewed the manuscript.

Declaration of interest. Authors declare no competing interests in relation to this work.

Keywords

MZF1; oncogene induced senescence; $p16^{INK4A}$; Ras; CHD7; non-small cell lung cancer; pancreatic adenocarcinoma

Introduction

Replicative senescence (RS) is a stable proliferative arrest resulted from exhaustion of replicative potential of normal cells [1]. Senescence can also be induced prematurely by cellular stresses, including oncogenes such as activated *ras* (termed oncogene induced senescence, or OIS) [1]. Senescence is accompanied by biomarkers, including senescence-associated-β-galactosidase (SA-β-Gal) activity, senescence-associated secretory phenotypes (SASP), senescence-associated heterochromatin foci (SAHF), telomere shortening, DNA damage responses, and altered expression of cell cycle inhibitors, such as $p16^{INK4A}$, p53 and $p21^{WAF1}$ [1–5]. $p16^{INK4A}$/retinoblastoma protein (RB) and p53/$p21^{WAF1}$ are two important effector pathways that cooperatively and independently regulate senescence [6, 7]. Senescence is also associated with global 3D genome reorganizations, such as impaired heterochromatic topologically associating domains (TADs) representing self-interacting genomic regions, altered genomic contacts and increased global chromosome density [8, 9].

Senescence is a double-edged sword in cancer development. OIS is a defense mechanism against malignant transformation, which suppresses proliferation of cells with activated oncogenes. In both human and mouse cancer models, senescence occurs in premalignant lesions associated with oncogenic mutations in K-*ras*, BRAF, PTEN and NF1, but is absent in malignant tumors [10, 11] [11, 12]. OIS thus represents a barrier to tumorigenesis, the disruption of which accelerates cancer development. On the other hand, senescent cells can enhance cancer development via SASP, which promotes formation of tumor amiable microenvironment [13–16]. Despite advancements in recent years, the signaling pathways that mediate senescence induction have not been fully delineated.

Myeloid zinc finger 1 (MZF1) is a member of the SCAN domain containing zinc finger transcriptional factor family. It functions as either a transcription activator or transcription repressor. There are two alternatively-spliced MZF1 isoforms in human [17–19]. The long isoform of MZF1 has 734 amino acids containing an N-terminal SCAN domain mediating dimerization or oligomerization, a linker regulatory region containing phosphorylation sites, and 13 C-terminal zinc finer (ZF) motifs that bind DNA [19, 20]. The 290-amino-acid short isoform consists of the SCAN domain and a regulatory domain that differs from that of the long isoform by an alternatively spliced exon, but without DNA binding domain. MZF1 was initially identified as a tumor suppressor in hematopoietic malignancy, as MZF1 knockout in mice promoted autonomous proliferation and long-term hemopoiesis in hemopoietic progenitor cells, and led to development of lethal neoplasias characterized by infiltration and disruption of liver architecture by cells of myeloid origin reminiscent of human chloromas [21]. In cultured cancer cells, MZF1 can either suppress [22–25] or promote [19–21, 26–31]

tumorigenic phenotypes such as cell proliferation, migration, invasion and xenograft tumor formation in a cancer type- and context-depend manner.

We reported previously that a transcriptional co-activator chromodomain helicase DNA binding protein 7 (CHD7) mediates oncogenic *ras*-induced senescence by inducing transcription of the $p16^{INK4A}$ gene upon binding to the $p16^{INK4A}$ promoter [32]. CHD7 is a chromatin remodeling factor with an ATP-dependent helicase activity, but without DNA binding domain[33]. It can be recruited to enhancers by methylated histone 3-Lys4 (H3K4me) or to promoters by transcription factors such as Oct4, Sox2, Sox9, Sox4, Sox11, Twist, p300 and PBAF [34–37]. In this study, we identified the long isoform of MZF1 as the transcriptional factor that recruits CHD7 to the $p16^{INK4A}$ promoter and as an essential mediator of oncogenic *ras*-induced $p16^{INK4A}$ transcription and senescence. Moreover, the expression of MZF1 is induced by oncogenic *ras* in senescent cells through c-Jun and Ets1 transcriptional factors upon their activation by the Ras-Raf-1-MEK-ERK pathway.

Activating mutations of K-*ras* are the most frequent mutations and initiating genetic event in pancreatic cancer, and also occur at high frequency (~30%) in non-small cell lung cancer (NSCLC) [11, 38, 39]. We found that MZF1 expression was reduced in tumors from patients with pancreatic adenocarcinoma (PAAD) or NSCLC as compared to normal tissues, and that reduced MZF1 expression correlated with poor survival in these patients. Thus, MZF1 is a potential tumor suppressor in PAAD and NSCLC. Analysis of single-cell RNA-sequencing data from PAAD patients revealed that MZF1 expression was reduced in tumor cells as compared to normal ductal cells, and that in tumor cells with intact RB1 expression, those with reduced MZF1 are more likely to express lower $p16^{INK4A}$, suggesting that loss of MZF1 expression is at least one mechanism responsible for inactivation of the $p16^{INK4A}$-RB pathway in PAAD.

Our findings have thus identified MZF1 as a novel regulator of $p16^{INK4A}$ and OIS, which may act as a tumor suppressor in certain cancers.

Results

MZF1 mediates oncogenic *ras*-induced recruitment of CHD7 to the $p16^{INK4A}$ promoter and CHD7-stimulated $p16^{INK4A}$ transcription

We previously reported that an ATP-dependent helicase CHD7 mediates oncogenic *ras*-induced $p16^{INK4A}$ transcription [32]. As CHD7 is a transcriptional coactivator without a DNA-binding domain [40], we hypothesize that CHD7 is recruited to the $p16^{INK4A}$ promoter by a transcription factor. We thus searched for the consensus binding sites for transcription factors in the 119 ~ +20 region containing the CHD7 binding peak [32] on the $p16^{INK4A}$ promoter, using the JASPAR database. We found that this region contained binding sites for multiple transcription factors (Table S1). In order to narrow down the candidates for the transcription factors that regulate $p16^{INK4A}$ transcription, we examined expression of these transcription factors and $p16^{INK4A}$ (CDKN2A) in senescent cells in datasets from the GEO database, including one data profile comparing replicative senescent cells and control growing cells and 8 profiles comparing cells undergoing oncogene-induced senescence and control growing cells. MZF1 was the only transcriptional factor consistently

upregulated together with CDKN2A/p16^{INK4A} in all these 9 GEO profiles (Fig. S1). We thus focused on MZF1 and investigated its role in oncogenic *ras*-induced p16^{INK4A} transcription and senescence.

We introduced either deletion or point mutations into the 3 MZF1 binding sites in a luciferase reporter driven by a 1kb p16^{INK4A} promoter (Fig. 1A), which was induced by CHD7 and oncogenic *ras* [32]. In 293T cells, deletions or point mutations of the MZF1 binding sites (Fig. 1B) and knockdown of MZF1 (Fig. 1C) reduced stimulation of transcription from the p16^{INK4A}-luciferase reporter by cotransfected CHD7, as compared to the reporter containing wild type MZF1 binding sites and the shRNA control (SC), respectively. Similarly, in BJ primary fibroblast cells stably transduced with the p16^{INK4A} luciferase reporters, oncogenic *ras* stimulated transcription for the wild type p16^{INK4A} promoter, which was abrogated by deletions or point mutations in the MZF1 binding sites (Fig. 1D). The MZF1 binding sites are thus required for *ras*- and CHD7-induced p16^{INK4A} transcription.

Using chromatin immunoprecipitation coupled with quantitative real time PCR (ChIP-qPCR), we showed that in BJ cells, both MZF1 and CHD7 were enriched in the −119 ~ +50 region of the p16^{INK4A} promoter, a region containing the previously identified CHD7 binding peak [32], and that binding of both proteins to this region was increased by oncogenic *ras* (Fig. 1E). Moreover, in BJ cells, CHD7 enrichment in the −119~+50 region of the p16^{INK4A} promoter was increased by the ectopically expressed long isoform of MZF1 (Fig. 1F). We constructed shRNAs silencing both long and short isoforms (sh-T1 and sh-T2), only the long isoform (sh-L), or only the short isoform (sh-S) of MZF1 (Fig. 1G–I). CHD7 enrichment in the −119~+50 region of the p16^{INK4A} promoter was decreased by shRNAs that silenced the expression of both isoforms (shT-1) or only the long isoform of MZF1 (shL) (Fig. 1J). CHD7 co-immunoprecipitated with MZF1 by an anti-MZF1 antibody, and MZF1 co-immunoprecipitated with CHD7 by an anti-CHD7 antibody (Fig. 1K), indicating that endogenous MZF1 and CHD7 interact with each other. The interaction between MZF1 and CHD7 was enhanced by oncogenic *ras*, likely because *ras* increased the expression of these proteins (Fig. 1K). Therefore, CHD7 is recruited to the p16^{INK4A} promoter by MZF1 upon *ras* activation.

Taken together, our results indicate that the ability of CHD7 to mediate *ras*-induced p16^{INK4A} transcription relies on its recruitment to the p16^{INK4A} promoter by MZF1.

MZF1 mediates oncogenic *ras*-induced p16^{INK4A} transcription.

We investigated the role of MZF1 in p16^{INK4A} transcription during OIS. Like oncogenic *ras*, ectopic expression of the long, but not the short, MZF1 (Fig. 2A–C), induced the expression of p16^{INK4A} mRNA and protein in BJ cells (Fig. 2D–E). While oncogenic *ras* induced p16^{INK4A} expression at both mRNA and protein levels, MZF1 shRNAs (sh-T1 and sh-T2) that knocked down both MZF1 isoforms (Fig. 1G–I, 2F) abrogated *ras*-induced p16^{INK4A} expression (Fig. 2G–H). Neither ectopic expression nor knockdown of MZF1 altered levels of total p53 or phosphorylation of p53 at Ser15, one of the key activation sites, in BJ cells with or without *ras* (Fig. 2E, H), suggesting that MZF1 specifically mediates induction of p16^{INK4A}, but not p53, by oncogenic *ras*.

Using $p16^{INK4A}$ promoter-driven luciferase reporters, we tested whether MZF1 mediated $p16^{INK4A}$ expression at the transcription level. In 293T cells, cotransfection of CHD7 or the long but not the short MZF1 stimulated transcription from the $p16^{INK4A}$ reporter (Fig. 2I). Induction of $p16^{INK4A}$ transcription by the long MZF1 was abolished by deletions or point mutations in the MZF1-binding sites on the $p16^{INK4A}$ promoter, while $p16^{INK4A}$ transcription in the presence of the short MZF1 was unaltered by the deletions or point mutations in the $p16^{INK4A}$ promoter (Fig. 2J–K). Moreover, in BJ cells, *ras*-induced transcription from the $p16^{INK4A}$ reporter was abrogated by deletions or point mutations of the MZF1-binding sites in the $p16^{INK4A}$ promoter (Fig. 1D) and by MZF1 shRNAs that silenced both isoforms (sh-T1) or the long isoform (sh-L) of MZF1 (Fig. 2L).

Thus, the long MZF1 isoform mediates *ras*-induced transcription of $p16^{INK4A}$.

MZF1 mediates oncogenic *ras*-induced senescence through CHD7.

Consistent with the importance of $p16^{INK4A}$ and p53 in senescence, *ras*-induced senescence was disrupted by the knockdown of $p16^{INK4A}$ or p53 (Fig. S2A–D). We thus investigated whether MZF1 was also important for *ras*-induced senescence. In control BJ cells (SC), *Ha-ras V12* induced proliferative arrest and accumulation of SA-β-gal, indicative of senescence induction; shRNAs silencing both long and short isoforms (sh-T1 and sh-T2) or only the long isoform (sh-L) of MZF1, but not that targeting the short isoform (sh-S) (Fig. 1G–I), abrogated *Ha-ras V12*-induced senescence (Fig. 3A–D), demonstrating that the long MZF1 is essential for OIS. Eectopic expression of the long (MZF1-L) but not the short (MZF1-S) MZF1 isoform also induced senescence, similar to *Ha-ras V12* (Fig. 3E–F).

Similar observations were made in HSAEC and primary human pancreatic cells (Fig. S3, S4), in that the long but not the short of MZF1 induced $p16^{INK4A}$ protein and mRNA levels and senescence (Fig. S3A–D, S4A–D), while the MZF1 shRNAs silencing both isoforms or only the long isoform, but not that silencing only the short isoform, abrogated *Ha-Ras V12*-induced $p16^{INK4A}$ expression and senescence (Fig. S3E–H, S4E–H)

Thus, the long MZF1 isoform is required for induction of $p16^{INK4A}$ expression and senescence by *ras*, and is also sufficient to induce $p16^{INK4A}$ expression and senescence, though its effect was not as robust as that of oncogenic *ras* (Fig. 3E–F), likely because posttranslational modifications, beside increased expression, induced by *ras* may also contribute to MZF1 function in senescence.

Furthermore, induction of senescence and $p16^{INK4A}$ expression by the long MZF1 was abrogated by knockdown of CHD7 in BJ cells (Fig. 3G–J), which indicates that MZF1 acts upstream of CHD7 to mediate senescence induction.

Oncogenic *ras* induces MZF1 expression through Raf1-MEK1-ERK.

Besides CHD7 [32], *Ha-ras V12* also increased expression of MZF1 isoforms at mRNA and protein levels in BJ cells (Fig. 4A–B), consistent with the upregulation of CDKN2A/$p16^{INK4A}$ and MZF1 in cells undergoing RS or OIS in GEO datasets (Fig. S1). Thus, *ras* may induce MZF1 expression, which in turn mediates $p16^{INK4A}$ transcription and senescence.

Global genome organization is altered in senescent cells and is associated with altered expression of senescence-regulating genes [8, 41, 42]. We analyzed the GSE118494 dataset containing in situ Hi-C and ChIP-seq data of growing IMR90 cells and those undergoing OIS, to profile DNA-DNA and DNA-protein interactions in chromosomal regions near the MZF1 and CDKN2A/p16^{INK4A} genes [8]. Analysis of the Hi-C data revealed that contact between the CDKN2A gene and its neighboring regions was significantly decreased in senescent cells compared to growing cells (Fig. S5A–B). The same trend was observed with the MZF1 gene (Fig. S5C–D). Thus, the chromatin structures surrounding MZF1 and CDKN2A/p16^{INK4A} genes are reorganized to a state consistent with active transcription in OIS cells [43].

Condensin II and cohesin are protein complexes consisting of structure maintenance of chromosomes (SMC) proteins, which regulate gene expression via high-order genome organization [41, 44]. Condesin II reinforces euchromatic A compartments where highly expressed genes are enriched, while the condensing II subunit CAP-H2 and cohesion (SMC1) are preferentially localized to active promoters and enhancers [8, 45]. In senescent cells, CAP-H2 and SMC1 are enriched at upregulated, senescence-associated genes, including those encoding SASP factors and p21^{WAF1}, as compared to proliferating cells, and are required for their upregulation and for senescence [8, 44]. Analysis of ChIP-seq data in GSE 118494 indicated that endogenous CAP-H2, ectopically expressed CAP-H2-FLAG and SMC1 were highly enriched near the CDKN2A and MZF1 genes in OIS cells, as compared to proliferating cells (Fig. S5E–F), consistent with the reported predominant localization of condensing II and cohesin at active promoters and enhancers [8, 46] and the higher CDKN2A and MZF1 expression in senescence cells than in proliferating cells (Fig. 4A–B, S1). Collectively, these results suggest that both MZF1 and CDKN2A/p16^{INK4A} genes are localized to chromosomal compartments undergoing active expression.

Oncogenic *ras* activates multiple downstream effector pathways, including Raf1-MEK-ERK, MKK3/6-p38, MKK4/7-JNK, and PI3K-AKT [40]. We analyzed the effects of constitutively active forms of these effectors [40] on MZF1 expression in BJ cells. Active Raf-1 and MEK1 induced expression of the long and short MZF1 isoforms at protein (Fig. 4C) and mRNA levels (Fig. 4D–E). In contrast, active MKK3, MKK4, MKK7, PI3K and AKT failed to increase the long MZF1 expression at protein or mRNA levels (Fig. 4C–D). Active MKK4, MKK7, PI3K and AKT increased expression of the short MZF1 (Fig. 4C, E), which does not contribute to *ras*-induced p16^{INK4A} expression or senescence (Fig. 2D–E, 2I, 3C–F). Moreover, a MEK1 inhibitor U0126 abrogated *ras*-induced upregulation of MZF1 and p16^{INK4A} (Fig. 4F). Thus, oncogenic *ras* induces MZF1 expression through the Raf-1-MEK-ERK pathway.

C-Jun and ETS1 are essential for *ras*-induced MZF1 transcription.

Previous studies showed that *ras* activates c-Jun and ETS1 transcription factors through phosphorylation mediated by MEK-ERK [47]. Indeed, in BJ cells, *Ha-ras V12* induced phosphorylation of c-Jun-S73 and ETS1-T38, the ERK substrate sites[47]; U0126 abrogated *ras*-induced phosphorylation of these sites (Fig. 4E), confirming that oncogenic *ras* induces c-Jun, and ETS1 phosphorylation in a MEK1/ERK-dependent fashion.

shRNA-mediated silencing of ETS1 (Fig. 5A–C) or c-Jun (Fig. 5D–F) disrupted induction of MZF1 expression by *ras* at both mRNA (Fig. 5B, E) and protein (Fig. 5C, F) levels in BJ cells. Ectopic expression of TAM67, a dominant negative c-Jun mutant lacking the transactivation domain but retaining the DNA binding domain [47], also reduced induction of MZF1 mRNA and protein by *Ha-ras V12* (Fig. 5G–H). Thus, c-Jun and ETS1 are required for *ras*-induced MZF1 expression.

To determine the roles of c-Jun and ETS1 on *ras*-induced MZF1 transcription, we constructed luciferase reporters driven by a 2.5 kb (−2512 ~ +130 relative to the TSS) or 1.5 kb (−1500 ~ +130) region of the MZF1 promoter (Fig. 6A). When co-transfected with *Ha-ras V12* into 293T cells, the 1.5 kb promoter was sufficient to mediate the *ras* responsiveness (Fig. 6B). We generated a retroviral luciferase reporter for the 1.5kb MZF1 promoter and transduced it into BJ cells to generate a stable MZF1 promoter reporter cell line. Knockdown of ETS1 or c-Jun (Fig. 6C) or ectopic expression of TAM67 (Fig. 6D) disrupted *ras*-induced transcription from this 1.5kb promoter, indicating requirement of c-Jun and ETS1 for *ras*-induced MZF1 transcription.

A search in JASPAR identified 2 c-Jun binding sites (c-Jun-A, −744 ~ −730 and c-Jun-B, −333 ~ −323) and 2 ETS1 binding sites (ETS1-A, −886 ~ −877 and ETS1-B, −256 ~ −247) in this 1.5 kb promoter region (Table S2, Fig. 6A). We analyzed c-Jun and ETS1 binding to these sites by ChIP-qPCR using primers amplifying the −900~−729 region containing c-Jun-A and ETS1-A and primers amplifying the −422~−242 region containing c-Jun-B and ETS1-B. ETS1 bound to ETS1-A, and c-Jun bound to both c-Jun-A and c-Jun-B in a *ras*-dependent manner, while ETS1 did not bind to ETS1-B either in the presence or absence of oncogenic *ras*, on the MZF1 promoter (Fig. 6E–F). Point mutations that disrupted the consensus binding sites in c-Jun-A, c-Jun-B, c-Jun-A-B or ETS1-A (Fig. 6A, Table S2) abrogated *Ha-ras V12*-inducted transcription from the stable 1.5kb-MZF1 promoter reporter in BJ cells (Fig. 6G).

Thus, oncogenic *ras* induces MZF1 transcription by activating the ETS1 and c-Jun transcriptional factors through the Raf-1-MEK1-ERK pathway.

MZF1 is a potential tumor suppressor in non-small lung cancer (NSCLC) and pancreatic adenocarcinoma (PAAD)

Analysis of data from the Cancer Genome Atlas (TCGA) database indicated downregulation of MZF1 expression in NSCLC, including lung adenocarcinoma (LUAD) and squamous cell carcinoma (LUSC) (Fig. 7A, S6), and other cancer types such as breast cancer (BRCA), head and neck cancer (HNSC), kidney chromophobe renal cell carcinoma (KICH), kidney papillary renal cell carcinoma (KIRP), and thyroid carcinoma (THCA) (Fig. S6), as compared to paired normal tissues.

Activating *ras* mutations occur in 30% of NSCLC patients and over 90% of PAAD patients, and are the drivers of these cancers [11, 38, 39]. We thus investigated the role of MZF1 in these 2 cancer types. Analysis of GEO data using Kaplan-Meier Plotter [48, 49] showed that low MZF1 expression correlated with poor survival in LUAD and LUSC patients (Fig. 7B). Since the RNA-seq data for PAAD in TCGA only included 4 normal tissues, we were

unable to determine confidently whether MZF1 expression was downregulated in PAAD. We thus compared MZF1 expression in patients at different disease stages based on initial diagnosis before treatments began. MZF1 expression was remarkable lower in patients with higher-stage (stages II and III/IV) diseases than in those with stage I disease (Fig. 7C). Moreover, analysis of 3 PAAD datasets (GSE101448, GSE62452 and GSE71729) from the GEO database revealed significant downregulation of MZF1 in PADD tissues as compared to paired normal tissues (Fig. 7D). Kaplan-Meier analysis of clinical data in TCGA showed correlation between low MZF1 expression and poor overall and disease free survival in PAAD patients (Fig. 7E). Results from these analyses of human patient data thus suggest that MZF1 may be a tumor suppresser in NSCLC and PAAD.

MZF1 and p16^{INK4A} expression are positively correlated in PAAD

We investigated whether reduced MZF1 expression contributes to p16^{INK4A} downregulation in human cancer. We failed to detect significant correlations between MZF1 and p16^{INK4A} expression in any cancer types in TCGA (Fig. S6B and data not shown). Surprisingly, p16^{INK4A} expression was upregulated or unchanged in tumors as compared to normal tissues in multiple cancers including LUAD, LUSC and PAAD in TCGA (Fig. S6C–D). Increased p16^{INK4A} expression has indeed been reported in malignant tumors of multiple cancers, likely due to loss of a negative feedback resulted from deregulation of RB1, the p16^{INK4A} downstream effector [50, 51]. RB1 loss correlated with high p16^{INK4A} expression in cancers such as breast cancer and lung cancer [50, 52–55].

To dissect the relationship between MZF1 and p16^{INK4A} expression among heterogeneous tumor cells from each patient and among different tumors with heterogeneous genetic backgrounds and treatment histories, we analyzed recently published single-cell RNA-sequencing (scRNA-seq) data from 24 PAAD samples from untreated patients and 11 healthy pancreases [56]. The original 57530 single cells were annotated as 10 different cell types based on known markers. We focused on the type 2 ductal cells that are the malignant ductal cells and the type 1 ductal cells that are the major normal origin of pancreatic tumor cells [56] (Fig. 8A).

Consistent with results from analyses of the TCGA and GEO datasets (Fig. 7D and S6C–D), MZF1 expression was lower, while p16^{INK4A} expression was higher, in type 2 (tumor) than in type 1 (normal) ductal cells (Fig. 8B–C). Moreover, RB1 expression was reduced in type 2 cells as compared to type 1 cells (Fig. 8D), and among the type 2 cells, high CDKN2A/p16^{INK4A} expression correlated with low RB1 expression (Fig. 8E). These findings were consistent with the previously reported inverse correlation between CDKN2A/p16^{INK4A} and RB1 expression, and suggested that in tumor cells with low RB1 expression, the CDKN2A/p16^{INK4A} level is increased due to loss of negative feedback and may no longer be relevant to cell proliferation since its downstream effector RB1 is already inactivated. After excluding the type 2 cells with lower-than-normal RB1 expression (Fig. 8F) from analyses, we found that low MZF1 expression indeed correlated with low CDKN2A/p16^{INK4A} expression in tumor cells with normal RB1 levels (Fig. 8G–I). Therefore, collectively, our data indicate that at least in some PAAD cells, such as those with normal RB1 levels,

decreased MZF1 expression may contribute to the reduction in CDKN2A/p16^{INK4A} and inactivation of the RB1 pathway, leading to disruption of senescence induction.

Discussion

In this study, we demonstrate that CHD7, a transcriptional co-activator without DNA binding domains, is recruited to the p16^{INK4A} promoter by a transcriptional factor MZF1, which mediates oncogenic *ras*-induced p16^{INK4A} transcription and senescence in a CHD7-dependent fashion. Further investigations revealed a novel signaling pathway mediating OIS and p16^{INK4A} expression, in which oncogenic *ras* activates the c-Jun and ETS1 transcription factors through phosphorylation mediated by the Raf-MEK-ERK cascade, which in turn stimulate transcription of the MZF1 gene, leading to increased MZF1 expression, enhanced CHD7 recruitment to the p16^{INK4A} promoter, elevated p16^{INK4A} expression, and senescence induction (Fig. 8J).

In NSCLC and PAAD, where activating *ras* mutations occur frequently [11, 38, 39], MZF1 expression is decreased in tumors as compared to normal tissues, and reduced MZF1 expression correlates with advanced disease stages and poor patient survival (Fig. 7A–E, S1), suggesting that MZF1 is a potential tumor suppressor in these cancers (Fig. 8J). Consistent with this notion, MZF1 mediates *ras*-induced p16^{INK4A} expression and senescence in primary human small airway lung epithelial cells and pancreatic epithelial cells, the origins of NSCLC and PAAD, respectively (Fig. S3A–H, S4A–H). Our initial attempt to determine the effect of MZF1 on p16^{INK4A} expression in human cancer was hindered by the lack of reduction (or even increase) in p16^{INK4A} expression in tumors with defective RB as reported previously, likely due to the loss of a negative feedback loop [50–55]. By focusing on single-cell RNA-seq data from untreated PAAD patients, we were able to demonstrate a correlation between reduced MZF1 levels and low p16^{INK4A} expression in tumor cells with normal RB levels, suggesting that decreased MZF1 expression contribute to cancer development through reduction in CDKN2A/p16^{INK4A} and inactivation of RB, at least in some PAAD tumor cells with functional RB.

Although oncogenic *ras* induced expression of both long and shout MZF1 isoforms, likely because they are derived from the same transcript, only the long isoform with DNA binding capacity [17–19] mediates *ras*-induced p16^{INK4A} transcription and senescence. Therefore, the DNA-binding activity is essential for the function of MZF1 in p16^{INK4A} transcription and senescence. Interestingly, while the long MZF1 isoform was essential for *ras*-induced p16^{INK4A} expression and senescence, its overexpression only partially mimicked the *ras* effects and induced moderate levels of senescence as compared to *ras* itself (Fig. 3E–F). It is likely that *ras*-induced posttranslational modifications, besides increased expression, is important for the role of MZF1 in senescence.

MZF1 expression can be regulated by transcription factors AP4 and c-Myb and by microRNAs including Let-7, miR-492, miR-337–3p in various biological settings in cancer cells [31, 57, 58]. Here, we identified a new regulatory pathway for MZF1 expression, in which oncogenic *ras* induced MZF1 transcription through the c-Jun and ETS1 upon their activation by the Raf1-MEK-ERK pathway. We previously reported that the same

Ras-Raf1-MEK-ERK-c-Jun/ETS1 axis stimulated transcription of p38δ that mediates OIS via a $p16^{INK4A}$/p53-independent mechanism [34]. Thus, in response to oncogenic *ras*, c-Jun and ETS1 are activated by Raf1-MEK-ERK and stimulate transcription of multiple targets that coordinate to mediate senescence induction.

Elevated $p16^{INK4A}$ level isa crucial for cellular senescence and tumor suppression [59, 60], and is a key effector in OIS (Fig. S2) [61]. It has been reported that transcriptional regulators such as Id1, YY1, PcG and YB1 suppress senescence by repressing $p16^{INK4A}$ transcription, while others including FOXA1, Sall2, ETS1/2 and histone H3K4 methyltransferase MLL1 bind to the p16 ^{INK4A} locus and induce $p16^{INK4A}$ during senescence [62]. Our study has identified MZF1 as a novel transcriptional factor essential for $p16^{INK4A}$ transcription during OIS. Since senescence is a barrier to oncogenic transformation and is mediated at least partly by $p16^{INK4A}$ [63, 64], regulators of $p16^{INK4A}$ are likely to control tumorigenesis. Indeed, loss of FOXA1 that mediates $p16^{INK4A}$ transcription leads to silencing of $p16^{INK4A}$, bypass of senescence, and *ras*-mediated oncogenic transformation in prostate and breast cancer cells [65]; up-regulated Id1 expression decreased $p16^{INK4A}$ expression, leading to increased proliferation in prostate cancer cells [66]. Investigations on the role of MZF1 in tumorigenesis is underway.

MZF1 is a multifaceted transcription factor that either promotes or suppresses tumorigenesis in a cancer type- and context-dependent fashion, likely by regulating different transcriptional targets under different conditions. MZF1 decreased viability, proliferation, migration, and anchorage-independence by inhibiting IGF-IR transcription in lymphoma cells [67], reduced transcription of the *Mtor* oncogene in both fibroblasts and mouse plasmacytoma cells [68], and suppressed migration and invasion of cervical cancer cells by inhibiting transcription of matrix metalloproteinase-2 [28]. These studies in cell culture are consistent with the cancer prone phenotype of the MZF1 knockout mice [21], suggesting that MZF1 is a tumor suppressor. On the other hand, silencing MZF1 suppressed migration, invasion and tumorigenicity by reducing PKCα expression in human hepatocellular carcinoma cells [22, 26], and overexpression of MZF1 in glioma cells induced cell proliferation and promoted growth of xenograft tumors implanted into mouse brains by inducing c-Myc transcription [69], suggesting a tumor promoting role of MZF1. The function MZF1 is controversial in some cancer types, likely due to differential experimental conditions. In breast cancer, MZF1 mediates invasion of Her2-positive cells by inducing expression of cysteine cathepsins B and L (CTSB and CTSL1) and PKCα [27, 70], and also inhibits brain metastasis of Her2 positive cancer cells by repressing βIII-tubulin expression [48]. In prostate cancer cells, MZF1 promotes tumorigenesis by up-regulating transcription of CDC37 [25], but also inhibits prostate cancer growth by inducing ferroportin transcription and ferroportin-driven iron egress [57]. The differential roles of MZF1 in cancer is consistent with our finding that MZF1 expression is upregulated in some, but downregulated in other, cancer types (Fig. S6A).

We found that MZF1 mediates OIS in primary HSAECs (Fig. S3), and that reduced MZF1 expression occurs in tumors from LUAD and LUSC patients and correlates with poor survival (Fig. 7A–B), suggesting that MZF1 suppresses NSCLC development. These results appears to contradict a previous report that MZF1 expression was increased in LUAD cells

as a result of loss of liver kinase B1 (LKB1), which in turn induced c-Myc expression, leading to enhanced anchorage-independent growth, migration and invasion of LUAD cells [24]. It is possible that this previously reported tumor-promoting activity of MZF1 operates mainly in LUAD cells with loss of LKB1. Similarly, reduction in MZF1 expression and correlation between reduced MZF1 levels and poor patient survival were observed in PAAD, another cancer type with high-frequency oncogenic *ras* mutations, suggesting that loss of MZF1 is crucial for abrogating oncogenic *ras*-induced $p16^{INK4A}$ expression and senescence, and that MZF1 is a tumor suppressor in cancers driven by activated *ras* mutations. However, we failed to observe correlations between *ras* mutations and reduced MZF1 expression and between reduced MZF1 expression and reduced $p16^{INK4A}$ expression in NSCLC and PAAD using TCGA data, likely due to heterogeneity among tumor cells from each patient and among different tumors with heterogeneous genetic backgrounds and treatment histories. We thus analyzed scRNA-seq data from untreated PAAD patients and normal individual [56], and found that upon exclusion of tumor cells with reduced RB1 expression, in which regulation of $p16^{INK4A}$ expression may no longer be relevant to cell proliferation and tumorigenesis due to inactivation of its downstream effector RB, reduced MZF1 expression indeed correlated with reduced $p16^{INK4A}$ expression, suggesting that at least in some PAAD tumor cells where $p16^{INK4A}$ is crucial, decreased MZF1 expression contributes to reduction in $p16^{INK4A}$ and thus inactivation of the RB pathway.

Of caution, most of our studies were performed using Ha-RasV12 and primary BJ fibroblast cells as models for senescence induction, which may differ from the oncogenic *K-ras* genes present in NSCLC and PAAD and primary lung and pancreatic epithelial cells, respectively. However, oncogenic *K-ras* also induces senescence[71, 72]. In addition, while most detailed mechanisms were studied in BJ cells, we showed that MZF1 mediates oncogenic *ras*-induced $p16^{INK4A}$ expression and senescence in primary human small airway epithelial cells (HSAECs) and primary human pancreatic epithelial cells (Fig. S3, S4). Thus, it is highly likely that the mechanistic insights obtained from the senescence models are relevant to specific cancers such as NSCLC and PAAD, although additional studies in more cancer specific systems are needed. Moreover, although analysis of the GEO data showed significant correlation between reduced MZF1 expression and poor survival in both LUAD and LUSC, analysis of the TCGA data showed a strong trend of opposite correlation in LUSC ($p=0.064$). The difference may lie in the different cohorts or different experimental approaches (gene chip vs RNA-seq) for generating data in the 2 databases.

In summary, our findings have identified a novel regulator of $p16^{INK4A}$ transcription, a new signaling component in the pathway that mediates OIS, and a mechanism underlying the tumor suppressing function of MZF1. Since MZF1 is a potential tumor suppressor in some cancers, the signaling pathway in which MZF1 exerts its function may serve as target for new anti-cancer therapies.

Materials and Methods

Cell lines and cell culture

BJ, HSAEC and primary human pancreatic epithelial cells were purchased from ATCC, Life Cell Technology and Cell Biologics, respectively. They were authenticated twice a year by

expression profiling and by mycoplasma tests. Senescence was analyzed as reported [32, 47]. Details are described in Supplemental Methods.

Plasmids.

Plasmids are described in Supplemental Methods.

Retrovirus- and lentivirus-mediated gene transduction.

Cells were transduced with recombinant retroviruses and lentiviruses as previously described [32] and selected as described in Supplemental Methods.

Western blot analysis.

Western blot was performed as described [32].

RNA isolation and quantitative Real-time PCR (qRT-PCR).

RNA was extracted and analyzed by qRT-PCR as described in Supplemental Methods using gene-specific primers (Table S3).

Luciferase reporter assay.

Luciferase reporters were reported previously [32] or generated as described in Supplemental Methods using primers in Table S3. Luciferase assays are described in Supplemental Methods.

ChIP-qPCR

Details of ChIP-qPCR are described in Supplemental Methods.

Genomic data analyses

Analyses of data from TCGA and GEO databases and single cell RNA-seq data are described in Supplemental Methods.

Statistical Analyses

Each experiments were performed in triplicates and repeated at least 3 times. Exact sample size, and methods and results from statistical analyses for each experiment are indicated in figure legends.

Supplementary Material

Refer to Web version on PubMed Central for supplementary material.

Acknowledgements

We thank the Cell Engineering and Cellular Imaging Shared Resources of WFBCCC. This study was supported by NIH/NCI grants CA131231, CA172115 and P30CA012197 (PS). PS is supported by the Anderson Oncology Research Professorship.

References

1. Gorgoulis V, Adams PD, Alimonti A, Bennett DC, Bischof O, Bishop C et al. Cellular Senescence: Defining a Path Forward. Cell 2019; 179: 813–827. [PubMed: 31675495]
2. Krizhanovsky V, Xue W, Zender L, Yon M, Hernando E, Lowe SW. Implications of cellular senescence in tissue damage response, tumor suppression, and stem cell biology. Cold Spring Harb Symp Quant Biol 2008; 73: 513–522. [PubMed: 19150958]
3. Lee S, Lee JS. Cellular senescence: a promising strategy for cancer therapy. BMB Rep 2019; 52: 35–41. [PubMed: 30526771]
4. Lee S, Schmitt CA. The dynamic nature of senescence in cancer. Nat Cell Biol 2019; 21: 94–101. [PubMed: 30602768]
5. Zhu J, Woods D, McMahon M, Bishop JM. Senescence of human fibroblasts induced by oncogenic Raf. Genes Dev 1998; 12: 2997–3007. [PubMed: 9765202]
6. Ferbeyre G, de Stanchina E, Lin AW, Querido E, McCurrach ME, Hannon GJ et al. Oncogenic ras and p53 cooperate to induce cellular senescence. Mol Cell Biol 2002; 22: 3497–3508. [PubMed: 11971980]
7. Sato M, Vaughan MB, Girard L, Peyton M, Lee W, Shames DS et al. Multiple oncogenic changes (K-RAS(V12), p53 knockdown, mutant EGFRs, p16 bypass, telomerase) are not sufficient to confer a full malignant phenotype on human bronchial epithelial cells. Cancer Res 2006; 66: 2116–2128. [PubMed: 16489012]
8. Iwasaki O, Tanizawa H, Kim KD, Kossenkov A, Nacarelli T, Tashiro S et al. Involvement of condensin in cellular senescence through gene regulation and compartmental reorganization. Nat Commun 2019; 10: 5688. [PubMed: 31831736]
9. Hernandez-Segura A, de Jong TV, Melov S, Guryev V, Campisi J, Demaria M. Unmasking Transcriptional Heterogeneity in Senescent Cells. Curr Biol 2017; 27: 2652–2660 e2654. [PubMed: 28844647]
10. Collado M, Serrano M. Senescence in tumours: evidence from mice and humans. Nat Rev Cancer 2010; 10: 51–57. [PubMed: 20029423]
11. di Magliano MP, Logsdon CD. Roles for KRAS in pancreatic tumor development and progression. Gastroenterology 2013; 144: 1220–1229. [PubMed: 23622131]
12. Courtois-Cox S, Jones SL, Cichowski K. Many roads lead to oncogene-induced senescence. Oncogene 2008; 27: 2801–2809. [PubMed: 18193093]
13. Hellmich C, Moore JA, Bowles KM, Rushworth SA. Bone Marrow Senescence and the Microenvironment of Hematological Malignancies. Front Oncol 2020; 10: 230. [PubMed: 32161723]
14. Liu XL, Ding J, Meng LH. Oncogene-induced senescence: a double edged sword in cancer. Acta Pharmacol Sin 2018; 39: 1553–1558. [PubMed: 29620049]
15. Ohtani N, Takahashi A, Mann DJ, Hara E. Cellular senescence: a double-edged sword in the fight against cancer. Exp Dermatol 2012; 21 Suppl 1: 1–4. [PubMed: 22626462]
16. Schosserer M, Grillari J, Breitenbach M. The Dual Role of Cellular Senescence in Developing Tumors and Their Response to Cancer Therapy. Front Oncol 2017; 7: 278. [PubMed: 29218300]
17. Peterson MJ, Morris JF. Human myeloid zinc finger gene MZF produces multiple transcripts and encodes a SCAN box protein. Gene 2000; 254: 105–118. [PubMed: 10974541]
18. Murai K, Murakami H, Nagata S. A novel form of the myeloid-specific zinc finger protein (MZF-2). Genes Cells 1997; 2: 581–591. [PubMed: 9413999]
19. Eguchi T, Prince T, Wegiel B, Calderwood SK. Role and Regulation of Myeloid Zinc Finger Protein 1 in Cancer. J Cell Biochem 2015; 116: 2146–2154. [PubMed: 25903835]
20. Brix DM, Bundgaard Clemmensen KK, Kallunki T. Zinc Finger Transcription Factor MZF1-A Specific Regulator of Cancer Invasion. Cells 2020; 9.
21. Gaboli M, Kotsi PA, Gurrieri C, Cattoretti G, Ronchetti S, Cordon-Cardo C et al. Mzf1 controls cell proliferation and tumorigenesis. Genes Dev 2001; 15: 1625–1630. [PubMed: 11445537]

22. Hsieh YH, Wu TT, Tsai JH, Huang CY, Hsieh YS, Liu JY. PKCalpha expression regulated by Elk-1 and MZF-1 in human HCC cells. Biochem Biophys Res Commun 2006; 339: 217–225. [PubMed: 16297876]
23. Liu X, Lei Q, Yu Z, Xu G, Tang H, Wang W et al. MiR-101 reverses the hypomethylation of the LMO3 promoter in glioma cells. Oncotarget 2015; 6: 7930–7943. [PubMed: 25829251]
24. Tsai LH, Wu JY, Cheng YW, Chen CY, Sheu GT, Wu TC et al. The MZF1/c-MYC axis mediates lung adenocarcinoma progression caused by wild-type lkb1 loss. Oncogene 2015; 34: 1641–1649. [PubMed: 24793789]
25. Eguchi T, Prince TL, Tran MT, Sogawa C, Lang BJ, Calderwood SK. MZF1 and SCAND1 Reciprocally Regulate CDC37 Gene Expression in Prostate Cancer. Cancers (Basel) 2019; 11.
26. Hsieh YH, Wu TT, Huang CY, Hsieh YS, Liu JY. Suppression of tumorigenicity of human hepatocellular carcinoma cells by antisense oligonucleotide MZF-1. Chin J Physiol 2007; 50: 9–15. [PubMed: 17593797]
27. Rafn B, Nielsen CF, Andersen SH, Szyniarowski P, Corcelle-Termeau E, Valo E et al. ErbB2-driven breast cancer cell invasion depends on a complex signaling network activating myeloid zinc finger-1-dependent cathepsin B expression. Mol Cell 2012; 45: 764–776. [PubMed: 22464443]
28. Tsai SJ, Hwang JM, Hsieh SC, Ying TH, Hsieh YH. Overexpression of myeloid zinc finger 1 suppresses matrix metalloproteinase-2 expression and reduces invasiveness of SiHa human cervical cancer cells. Biochem Biophys Res Commun 2012; 425: 462–467. [PubMed: 22846578]
29. Deng Y, Wang J, Wang G, Jin Y, Luo X, Xia X et al. p55PIK transcriptionally activated by MZF1 promotes colorectal cancer cell proliferation. Biomed Res Int 2013; 2013: 868131. [PubMed: 23509792]
30. Lee JH, Kim SS, Lee HS, Hong S, Rajasekaran N, Wang LH et al. Upregulation of SMAD4 by MZF1 inhibits migration of human gastric cancer cells. Int J Oncol 2017; 50: 272–282. [PubMed: 27922669]
31. Li GQ, He Q, Yang L, Wang SB, Yu DD, He YQ et al. Clinical Significance of Myeloid Zinc Finger 1 Expression in the Progression of Gastric Tumourigenesis. Cell Physiol Biochem 2017; 44: 1242–1250. [PubMed: 29179204]
32. Su W, Hong L, Xu X, Huang S, Herpai D, Li L et al. miR-30 disrupts senescence and promotes cancer by targeting both p16(INK4A) and DNA damage pathways. Oncogene 2018; 37: 5618–5632. [PubMed: 29907771]
33. Feng W, Shao C, Liu HK. Versatile Roles of the Chromatin Remodeler CHD7 during Brain Development and Disease. Front Mol Neurosci 2017; 10: 309. [PubMed: 29033785]
34. Feng W, Khan MA, Bellvis P, Zhu Z, Bernhardt O, Herold-Mende C et al. The chromatin remodeler CHD7 regulates adult neurogenesis via activation of SoxC transcription factors. Cell Stem Cell 2013; 13: 62–72. [PubMed: 23827709]
35. Bajpai R, Chen DA, Rada-Iglesias A, Zhang J, Xiong Y, Helms J et al. CHD7 cooperates with PBAF to control multipotent neural crest formation. Nature 2010; 463: 958–962. [PubMed: 20130577]
36. Schnetz MP, Handoko L, Akhtar-Zaidi B, Bartels CF, Pereira CF, Fisher AG et al. CHD7 targets active gene enhancer elements to modulate ES cell-specific gene expression. PLoS Genet 2010; 6: e1001023. [PubMed: 20657823]
37. Engelen E, Akinci U, Bryne JC, Hou J, Gontan C, Moen M et al. Sox2 cooperates with Chd7 to regulate genes that are mutated in human syndromes. Nat Genet 2011; 43: 607–611. [PubMed: 21532573]
38. Roman M, Baraibar I, Lopez I, Nadal E, Rolfo C, Vicent S et al. KRAS oncogene in non-small cell lung cancer: clinical perspectives on the treatment of an old target. Mol Cancer 2018; 17: 33. [PubMed: 29455666]
39. Waters AM, Der CJ. KRAS: The Critical Driver and Therapeutic Target for Pancreatic Cancer. Cold Spring Harb Perspect Med 2018; 8.
40. Schnetz MP, Bartels CF, Shastri K, Balasubramanian D, Zentner GE, Balaji R et al. Genomic distribution of CHD7 on chromatin tracks H3K4 methylation patterns. Genome Res 2009; 19: 590–601. [PubMed: 19251738]

41. Sun L, Yu R, Dang W. Chromatin Architectural Changes during Cellular Senescence and Aging. Genes (Basel) 2018; 9.
42. Yokoyama Y, Zhu H, Zhang R, Noma K. A novel role for the condensin II complex in cellular senescence2015; 14: 2160–2170.
43. Ulianov SV, Khrameeva EE, Gavrilov AA, Flyamer IM, Kos P, Mikhaleva EA et al. Active chromatin and transcription play a key role in chromosome partitioning into topologically associating domains. Genome Res 2016; 26: 70–84. [PubMed: 26518482]
44. Yokoyama Y, Zhu H, Zhang R, Noma K. A novel role for the condensin II complex in cellular senescence. Cell Cycle 2015; 14: 2160–2170. [PubMed: 26017022]
45. Li W, Hu Y, Oh S, Ma Q, Merkurjev D, Song X et al. Condensin I and II Complexes License Full Estrogen Receptor alpha-Dependent Enhancer Activation. Mol Cell 2015; 59: 188–202. [PubMed: 26166704]
46. Kagey MH, Newman JJ, Bilodeau S, Zhan Y, Orlando DA, van Berkum NL et al. Mediator and cohesin connect gene expression and chromatin architecture. Nature 2010; 467: 430–435. [PubMed: 20720539]
47. Kwong J, Chen M, Lv D, Luo N, Su W, Xiang R et al. Induction of p38delta expression plays an essential role in oncogenic ras-induced senescence. Mol Cell Biol 2013; 33: 3780–3794. [PubMed: 23878395]
48. Kanojia D, Panek WK, Cordero A, Fares J, Xiao A, Savchuk S et al. BET inhibition increases betaIII-tubulin expression and sensitizes metastatic breast cancer in the brain to vinorelbine. Sci Transl Med 2020; 12.
49. Gyorffy B, Lanczky A, Eklund AC, Denkert C, Budczies J, Li Q et al. An online survival analysis tool to rapidly assess the effect of 22,277 genes on breast cancer prognosis using microarray data of 1,809 patients. Breast Cancer Res Treat 2010; 123: 725–731. [PubMed: 20020197]
50. Romagosa C, Simonetti S, Lopez-Vicente L, Mazo A, Lleonart ME, Castellvi J et al. p16(Ink4a) overexpression in cancer: a tumor suppressor gene associated with senescence and high-grade tumors. Oncogene 2011; 30: 2087–2097. [PubMed: 21297668]
51. Schwartz B, Avivi-Green C, Polak-Charcon S. Sodium butyrate induces retinoblastoma protein dephosphorylation, p16 expression and growth arrest of colon cancer cells. Mol Cell Biochem 1998; 188: 21–30. [PubMed: 9823007]
52. Herschkowitz JI, He X, Fan C, Perou CM. The functional loss of the retinoblastoma tumour suppressor is a common event in basal-like and luminal B breast carcinomas. Breast Cancer Res 2008; 10: R75. [PubMed: 18782450]
53. Dublin EA, Patel NK, Gillett CE, Smith P, Peters G, Barnes DM. Retinoblastoma and p16 proteins in mammary carcinoma: their relationship to cyclin D1 and histopathological parameters. Int J Cancer 1998; 79: 71–75. [PubMed: 9495362]
54. Gorgoulis VG, Zacharatos P, Kotsinas A, Liloglou T, Kyroudi A, Veslemes M et al. Alterations of the p16-pRb pathway and the chromosome locus 9p21–22 in non-small-cell lung carcinomas: relationship with p53 and MDM2 protein expression. Am J Pathol 1998; 153: 1749–1765. [PubMed: 9846966]
55. Bastide K, Guilly MN, Bernaudin JF, Joubert C, Lectard B, Levalois C et al. Molecular analysis of the Ink4a/Rb1-Arf/Tp53 pathways in radon-induced rat lung tumors. Lung Cancer 2009; 63: 348–353. [PubMed: 18656278]
56. Peng J, Sun BF, Chen CY, Zhou JY, Chen YS, Chen H et al. Single-cell RNA-seq highlights intra-tumoral heterogeneity and malignant progression in pancreatic ductal adenocarcinoma. Cell Res 2019; 29: 725–738. [PubMed: 31273297]
57. Chen Y, Zhang Z, Yang K, Du J, Xu Y, Liu S. Myeloid zinc-finger 1 (MZF-1) suppresses prostate tumor growth through enforcing ferroportin-conducted iron egress. Oncogene 2015; 34: 3839–3847. [PubMed: 25284586]
58. Tvingsholm SA, Hansen MB, Clemmensen KKB, Brix DM, Rafn B, Frankel LB et al. Let-7 microRNA controls invasion-promoting lysosomal changes via the oncogenic transcription factor myeloid zinc finger-1. Oncogenesis 2018; 7: 14. [PubMed: 29396433]
59. LaPak KM, Burd CE. The molecular balancing act of p16(INK4a) in cancer and aging. Mol Cancer Res 2014; 12: 167–183. [PubMed: 24136988]

60. Coppe JP, Rodier F, Patil CK, Freund A, Desprez PY, Campisi J. Tumor suppressor and aging biomarker p16(INK4a) induces cellular senescence without the associated inflammatory secretory phenotype. J Biol Chem 2011; 286: 36396–36403. [PubMed: 21880712]

61. Serrano M, Lin AW, McCurrach ME, Beach D, Lowe SW. Oncogenic ras provokes premature cell senescence associated with accumulation of p53 and p16INK4a. Cell 1997; 88: 593–602. [PubMed: 9054499]

62. Kotake Y, Naemura M, Murasaki C, Inoue Y, Okamoto H. Transcriptional Regulation of the p16 Tumor Suppressor Gene. Anticancer Res 2015; 35: 4397–4401. [PubMed: 26168478]

63. Brookes S, Rowe J, Ruas M, Llanos S, Clark PA, Lomax M et al. INK4a-deficient human diploid fibroblasts are resistant to RAS-induced senescence. EMBO J 2002; 21: 2936–2945. [PubMed: 12065407]

64. Braig M, Lee S, Loddenkemper C, Rudolph C, Peters AH, Schlegelberger B et al. Oncogene-induced senescence as an initial barrier in lymphoma development. Nature 2005; 436: 660–665. [PubMed: 16079837]

65. Zhang Y, Tong T. FOXA1 antagonizes EZH2-mediated CDKN2A repression in carcinogenesis. Biochem Biophys Res Commun 2014; 453: 172–178. [PubMed: 25264199]

66. Ouyang XS, Wang X, Ling MT, Wong HL, Tsao SW, Wong YC. Id-1 stimulates serum independent prostate cancer cell proliferation through inactivation of p16(INK4a)/pRB pathway. Carcinogenesis 2002; 23: 721–725. [PubMed: 12016143]

67. Vishwamitra D, Curry CV, Alkan S, Song YH, Gallick GE, Kaseb AO et al. The transcription factors Ik-1 and MZF1 downregulate IGF-IR expression in NPM-ALK(+) T-cell lymphoma. Mol Cancer 2015; 14: 53. [PubMed: 25884514]

68. Zhang S, Shi W, Ramsay ES, Bliskovsky V, Eiden AM, Connors D et al. The transcription factor MZF1 differentially regulates murine Mtor promoter variants linked to tumor susceptibility. J Biol Chem 2019; 294: 16756–16764. [PubMed: 31548308]

69. Li J, Liao T, Liu H, Yuan H, Ouyang T, Wang J et al. Hypoxic Glioma Stem Cell-Derived Exosomes Containing Linc01060 Promote Progression of Glioma by Regulating the MZF1/c-Myc/HIF1alpha Axis. Cancer Res 2021; 81: 114–128. [PubMed: 33158815]

70. Brix DM, Tvingsholm SA, Hansen MB, Clemmensen KB, Ohman T, Siino V et al. Release of transcriptional repression via ErbB2-induced, SUMO-directed phosphorylation of myeloid zinc finger-1 serine 27 activates lysosome redistribution and invasion. Oncogene 2019; 38: 3170–3184. [PubMed: 30622337]

71. Scaglioni PP, Rabellino A, Yung TM, Bernardi R, Choi S, Konstantinidou G et al. Translation-dependent mechanisms lead to PML upregulation and mediate oncogenic K-RAS-induced cellular senescence. EMBO Mol Med 2012; 4: 594–602. [PubMed: 22359342]

72. Campisi J, d'Adda di Fagagna F. Cellular senescence: when bad things happen to good cells. Nat Rev Mol Cell Biol 2007; 8: 729–740. [PubMed: 17667954]

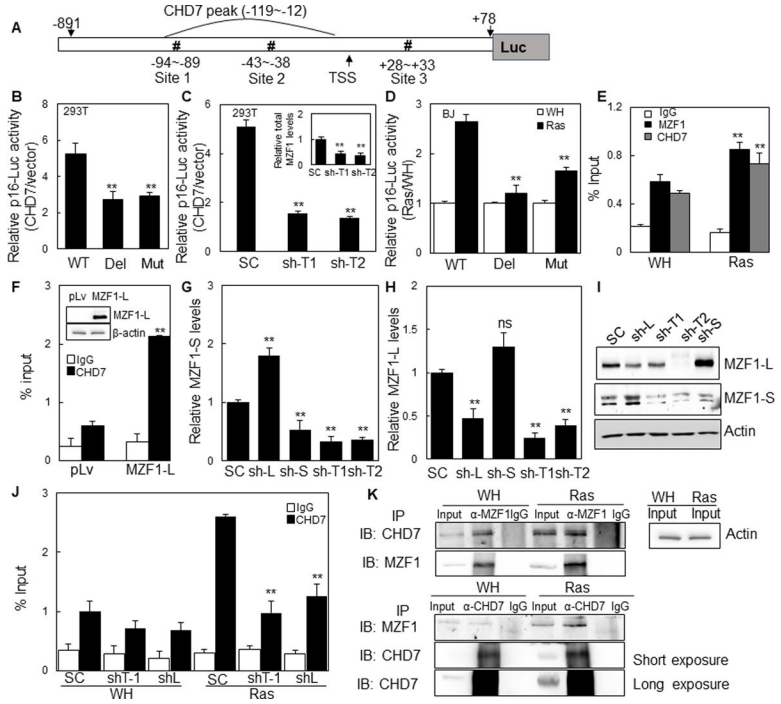

Fig. 1. MZF1 mediates oncogenic *ras*-induced recruitment of CHD7 to the p16^{INK4A} promoter and CHD7-stimulated p16^{INK4A} transcription.

(A) A diagram of the p16^{INK4A} promoter luciferase reporter used in the study, showing the CHD7 binding peak (−119 ~ −12), MZF1 binding sites (site 1–3, #) and transcription start site (TSS).

(B) The p16^{INK4A} promoter luciferase reporter with wild type MZF1 binding sites (WT) or with deletion mutations (Del) or point mutations (Mut) in the MZF1 binding sites were transfected to 293T cells with pcCDNA3-CHD7 or vector.

(C) The wild type p16^{INK4A} promoter luciferase reporter was transfected with pCDNA3-CHD7 or vector into 293T cells transduced with shRNA control (SC) or MZF1 shRNAs targeting both long and short isoforms (sh-T1 and sh-T2). Insert shows knockdown efficiency of the shRNAs, measured by qRT-PCR.

(D) BJ cells stably transduced with the wild type p16^{INK4A} promoter reporter (WT) or that containing deletion mutations (Del) or point mutations (Mut) in the MZF1 binding sites were transduced with HaRasV12 (Ras) or vector (WH).

(B-D) Luciferase activity was measured 48h after transfection (B-C) or 7 days after *ras* transduction (D) and normalized to protein concentrations determined by BCA assays. Relative p16-Luc activity was calculated by dividing values of CHD7 or Ras cells by that of vector control cells. Values are means±SDs for triplicates. ** $p < 0.01$ vs WT (B, D) or SC (C) in Student's t test.

(E) Chromatin was immunoprecipitated from BJ cells transduced with HaRasV12 (Ras) or vector (WH) using an anti-CHD7 or anti-MZF1 antibody or control IgG (rabbit IgG).

(F) Chromatin was immunoprecipitated from BJ cells transduced with the long MZF1 isoform (MZF1-L) or vector (pLv) using an anti-CHD7 antibody or control IgG (rabbit IgG). Insert shows overexpression of the long MZF1 isoform as determined by Western blotting.

(E-F) DNA present in immunoprecipitated complexes was quantified by real-time PCR using primers that amplify the −119 ~ +50 region of $p16^{INK4A}$ promoter and normalized to input. Values are means±SDs for triplicates. ** $p < 0.01$ vs vector (WH or pLv) by Student's t test.

(G-H) Expression levels of the short (G) and long (H) MZF1 isoforms in BJ cells transduced with shRNA control (SC) or shRNAs specific for the long (sh-L), short (sh-S) or both (sh-T1 and sh-T2) isoforms, as determined by qRT-PCR. Values are means±SDs for triplicates. ns, not significant, $p > 0.05$; ** $p < 0.01$ vs SC by Student's t test.

(I) Expression levels of the MZF1 isoforms in BJ cells transduced with shRNA control (SC) or shRNAs specific for the long (sh-L), short (sh-S) or both (sh-T1 and sh-T2) isoforms, as determined by Western blot analysis.

(J) Chromatin was immuneprecipitated from BJ cells transduced with shRNA control (SC) or MZF1 shRNAs targeting both isoforms (sh-T1) or the long isoform (sh-L) and with HaRasV12 (Ras) or vector (WH), using an anti-CHD7 antibody or control rabbit IgG (IgG). DNA present in immunoprecipitated complexes was quantified by real-time PCR using primers that amplify the −119 ~ +50 region of the $p16^{INK4A}$ promoter and normalized to input. Values are means±SDs for triplicates. ** $p < 0.01$ vs SC by Student's t test.

(K) Western blot analysis of CHD7 and MZF1 co-immunoprecipitated by an anti-MZF1 antibody or control IgG (top) or an anti-CHD7 antibody or control IgG (bottom) from BJ cells transduced with HaRasV12 (Ras) or vector (WH).

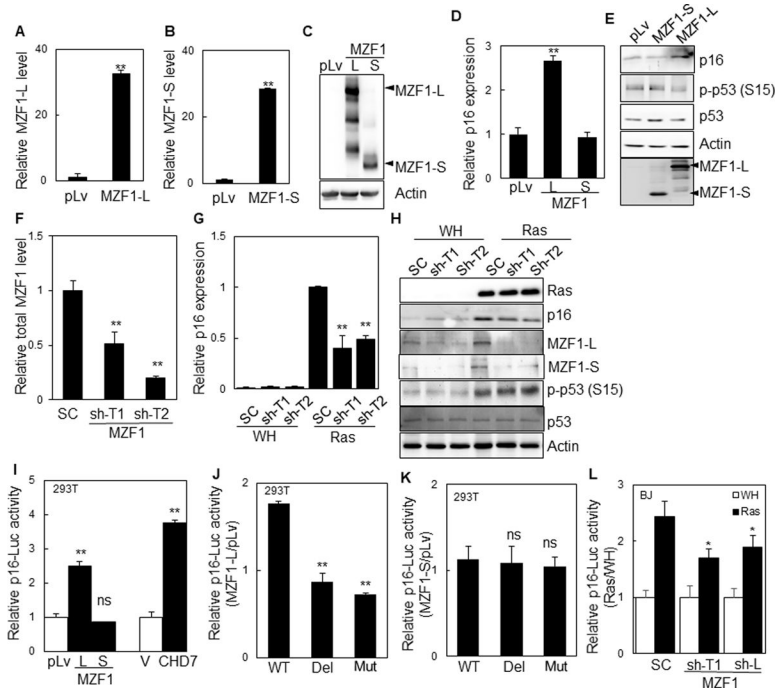

Fig. 2. The long MZF1 isoform mediates oncogenic *ras*-induced p16^{INK4A} transcription.

(A-C) BJ cells transduced with the long (MZF1-L) or short (MZF1-S) MZF1 isoform or vector (pLv) were analyzed for MZF1 expression by qRT-PCR (A and B, for the long and short isoforms, respectively) and Western blotting (C). Values are means±SDs for triplicates. ** $p<0.01$ vs pLv by Student's t test.

(D-E) BJ cells transduced with the long (MZF1-L) or short (MZF1-S) MZF1 isoform or vector (pLv) were analyzed for p16^{INK4A} mRNA levels by qRT-PCR (D) and for p16^{INK4A} and phospho- and total p53 proteins by Western blotting (E). Values are means±SDs for triplicates. ** $p < 0.01$ vs pLv by Student's t test.

(F) BJ cells transduced with shRNA control (SC) or shRNAs targeting both MZF1 isoforms (sh-T1 and sh-T2) were analyzed for knockdown efficiency by qRT-PCR. Values are means±SDs for triplicates. ** $p < 0.01$ vs SC by Student's t test.

(G-H) BJ cells transduced with shRNA control (SC) or shRNAs targeting both MZF1 isoforms (sh-T1 and sh-T2) and HaRasV12 (Ras) or vector (WH) were analyzed p16^{INK4A} mRNA level by qRT-PCR (G) and protein levels by Western blotting (E). Values are means±SDs for triplicates. ** $p < 0.01$ vs SC by Student's t test.

(I) The wild type p16^{INK4A} promoter luciferase reporter was co-transfected with the long (MZF1-L) or short (MZF1-S) MZF1 isoform, CHD7 or vector (pLv or V) into 293T cells.

(J-K) The wild type (WT) p16^{INK4A} promoter luciferase reporter or that with deletion mutations (Del) or point mutations (Mut) in the MZF1 binding was transfected into 293T cells with the long (MZF1-L) (J) or short (MZF1-S) (K) MZF1 isoform.

(L) BJ cells stably transduced with the wild type p16^{INK4A} promoter luciferase reporter was transduced with shRNA control (SC) or MZF1 shRNAs (sh-T1 and sh-L).

(I-L) Luciferase activity was measured 48h after transfection (I-K) or 7 days after *ras* transduction (L) and normalized to protein concentrations determined by BCA assays. Relative p16-luc activity was calculated by dividing values of MZF1-L, MZF1-S, CHD7

or Ras cells by that of vector control cells. Values are means±SDs for triplicates. ns, not significant, $p > 0.05$; * $p < 0.05$; ** $p < 0.01$ vs pLv (I), WT (J-K) or SC (L) by Student's t test.

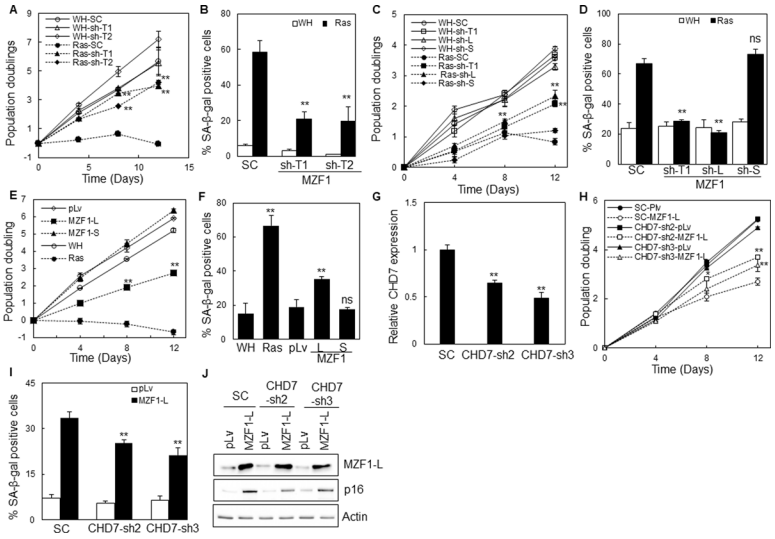

Fig. 3. MZF1 mediates oncogenic *ras*-induced senescence through CHD7.

(A) Growth curves of BJ cells transduced with shRNA control (SC) or shRNAs targeting both MZF1 isoforms (sh-T1 and sh-T2) and HaRasV12 (Ras) or vector (WH).

(B) Percentage of SA-β-Gal positive cells in populations in (A) on day-12 of the growth curves.

(C) Growth curves of BJ cells transduced with shRNA control (SC) or MZF1 shRNAs targeting both isoforms (sh-T1), or the long (sh-L) or short (sh-S) isoform, and HaRasV12 (Ras) or vector (WH).

(D) Percentage of SA-β-Gal positive cells in populations in (C) on day-12 of the growth curves.

(E) Growth curves of BJ cells transduced with the long (MZF1-L) or short (MZF1-S) MZF1 isoforms or vector (pLv).

(F) Percentage of SA-β-Gal positive cells in populations in (E) on day-12 of the growth curves.

(G) BJ cells transduced with shRNAs for CHD7 or shRNA control (SC) were analyzed for knockdown efficiency by qRT-PCR.

(H) Growth curves of BJ cells transduced with control shRNA (SC) or CHD7 shRNAs (sh2 and sh3) and the long MZF1 isoform (MZF1-L) or vector (pLv).

(I) Percentage of SA-β-Gal positive cells in populations in (H) on day-12 of the growth curves.

(A-I) Values are means±SDs for triplicates. ns, not significant, $p > 0.05$; ** $p < 0.01$ vs SC-Ras (A-D), WH/pLv (E-F), SC (G) or SC-MZF1-L (H-I) by Student's t test.

(J) BJ cells transduced with control shRNA (SC) or CHD7 shRNAs (sh2 and sh3) and the long MZF1 isoform (MZF1-L) or vector (pLv) were analyzed for $p16^{INK4A}$ expression by Western blotting.

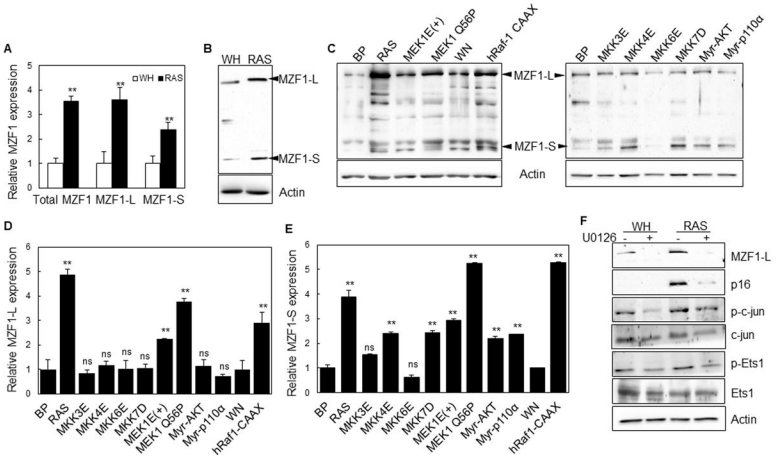

Fig. 4. Oncogenic *ras* induces MZF1 expression through the Raf1-MEK1-ERK pathway.

(A-B) BJ cells transduced with HaRasV12 (Ras) or vector (WH) were measured for MZF1 mRNA and protein levels by qRT-PCR (A) and Western blotting (B), respectively. Positions of the long (MZF1-L) and short (MZF1-S) MZF1 isoforms are marked by arrows.

(C) Western blot analysis of MZF1 levels in BJ cells on day-12 after transduction of HaRasV12 (Ras), constitutively active forms of the indicated Ras downstream effectors, or vector controls (BP or WN). Positions of the long (MZF1-L) and short (MZF1-S) MZF1 isoforms are marked by arrows.

(D-E) Cells in (C) were measured for the mRNA levels of the long (MZF1-L) (D) and short (MZF1-S) (E) MZF1 isoforms by qRT-PCR.

(F) Western blot analysis of BJ cells transduced with HaRasV12 (Ras) or vector (WH) and treated with 10 μM of U0126 or vehicle for 24h starting on day-10 after *ras* transduction.

(A, D-E) Values are means±SDs for triplicates. ns, not significant, $p > 0.05$; **$p<0.01$ vs WH (A) or BP/WN (D-E) by Student's t test.

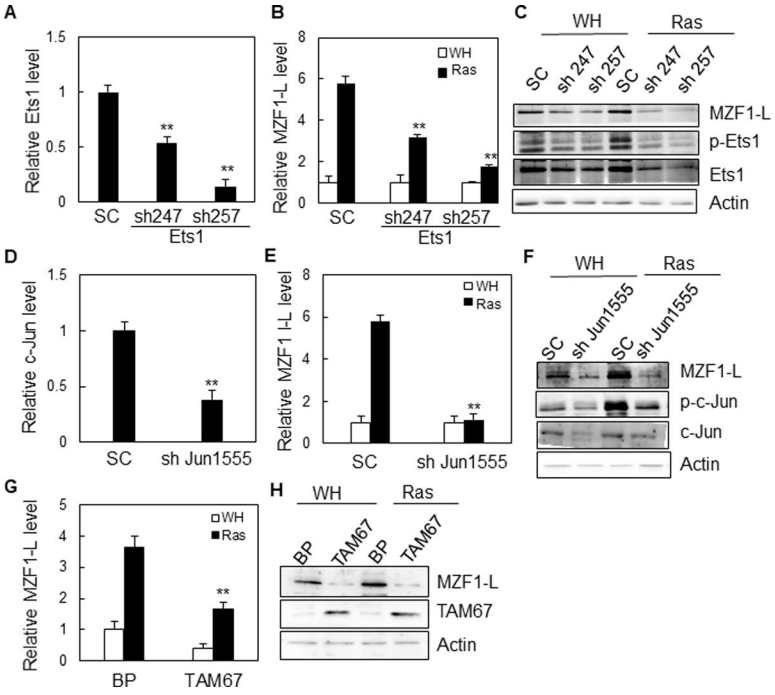

Fig. 5. Oncogenic *ras*-induced MZF1 transcription requires c-Jun and Ets1.

(A) Relative Ets1 mRNA levels in BJ cells transduced with shRNA control (SC) or ETS1 shRNAs (sh247 and sh257) as measured by qRT-PCR.

(B-C) BJ cells transduced with a shRNA control (SC) or Ets1 shRNAs (sh247 and sh257) and HaRasV12 (Ras) or vector (WH) were measured for MZF1 mRNA and protein levels by qRT-PCR (B) and Western blotting (C), respectively, on day-10 after *ras* transduction.

(D) Relative c-Jun mRNA levels in BJ cells transduced with shRNA control (SC) or a c-Jun shRNA (shJun1555) as measured by qRT-PCR.

(E-F) BJ cells transduced with a shRNA control (SC) or a c-Jun shRNA (shJun1555) and HaRasV12 (Ras) or vector (WH) were measured for MZF1 (MZF1-L) mRNA and protein levels by qRT-PCR (E) and Western blotting (F), respectively, on day-10 after *ras* transduction.

(G-H) BJ cells transduced with a dominant negative mutant of c-Jun (TAM67) or vector (BP) and HaRasV12 (Ras) or vector (WH) were measured for MZF1 (MZF1-L) mRNA and protein levels by qRT-PCR (G) and Western blotting (H), respectively, on day-10 after *ras* transduction.

(A-B, D-E, G) Values are means±SDs for triplicates. ** $p < 0.01$ vs SC (A, D), SC-Ras (B, E) or BP-Ras (G) by Student's t test.

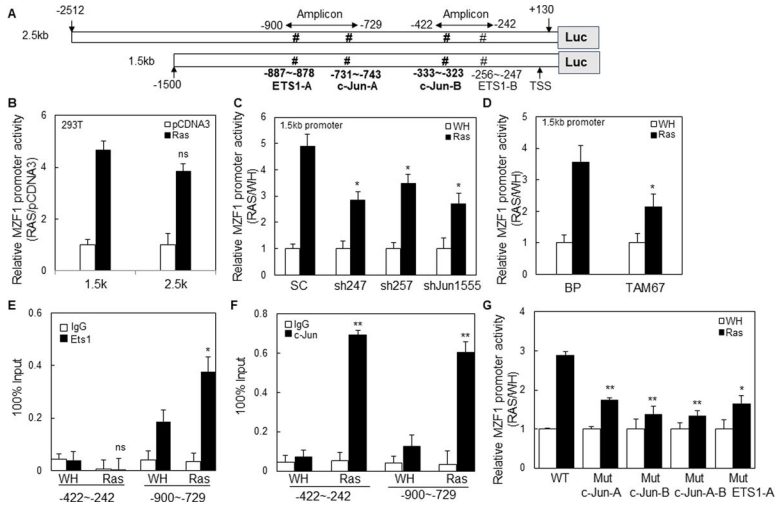

Fig. 6. The c-Jun and Ets1 binding sites on the MZF1 promoter are required for oncogenic *ras*-induced MZF1 transcription.

(A) Diagrams of the MZF1 promoter luciferase reporters used in the study, showing positions of the predicted ETS1 (ETS1-A and ETS1-B) and c-Jun binding sites (c-Jun-A and c-Jun-B), the transcriptional start site (TSS), and the amplicons used in ChIP-qPCR in (E-F). The actual ETS1 and c-Jun binding sites (ETS1-A, c-Jun-A and c-Jun-B) confirmed by ChIP are shown in bold.

(B) 293T cells were co-transfected with the 2.5kb or 1.5kb MZF1 promoter reporter and pCDNA3-HaRasV12 (Ras) or vector (pCDNA3).

(C-D) BJ cells stably transduced with the 1.5kb MZF1 promoter reporter were transduced with a shRNA control (SC) or shRNAs for ETS1 (sh247 and 257) or Jun (shJun1555), or TAM67 or vector (BP), and HaRasV12 (Ras) or vector (WH).

(B-D) Luciferase activity was measured 48h (B) or 10 days (C-D) after *ras* transfection (B) or transduction (C-D) and normalized to protein concentrations determined by BCA assays. Relative MZF1 promoter activity was calculated by dividing values of Ras cells by that of vector (pCDNA3 or WH) cells

(E-F) ChIP analysis of Ets1 and c-Jun binding to the MZF1 promoter. Chromatin was immunoprecipitated from BJ cells transduced with HaRasV12 (Ras) or vector (WH) using an anti-ETS1 (E) or anti-c-Jun (F) antibody or control rabbit IgG (IgG). DNA present in immunoprecipitated complexes was quantified by qPCR using primers amplifying the −900~−729 and −422~−242 regions (A) of the MZF1 promoter and normalized to inputs.

(G) BJ cells stably transduced with the wild type 1.5kb MZF1 promoter reporter (WT) or that containing point mutations in the c-Jun binding sites (MUT-c-Jun-A, MUT-c-Jun-B and MUT-c-Jun-A-B) or the ETS1 binding site (MUT-ETS1-A) were transduced HaRasV12 (Ras) or vector (WH). Luciferase activity was measured 10 days after *ras* transduction and normalized to protein concentrations determined by BCA assays. Relative MZF1 promoter activity was calculated by dividing values of Ras cells by that of WH cells.

(B-G) Values are means±SDs for triplicates. ns, not significant, $p > 0.05$; *$p < 0.05$; ** $p < 0.01$ vs 1.5k-Ras (B), SC-Ras (C), BP-Ras (D), WH-Ets1 (E), WH-c-Jun (F) or WT-Ras (G) by Student's t test.

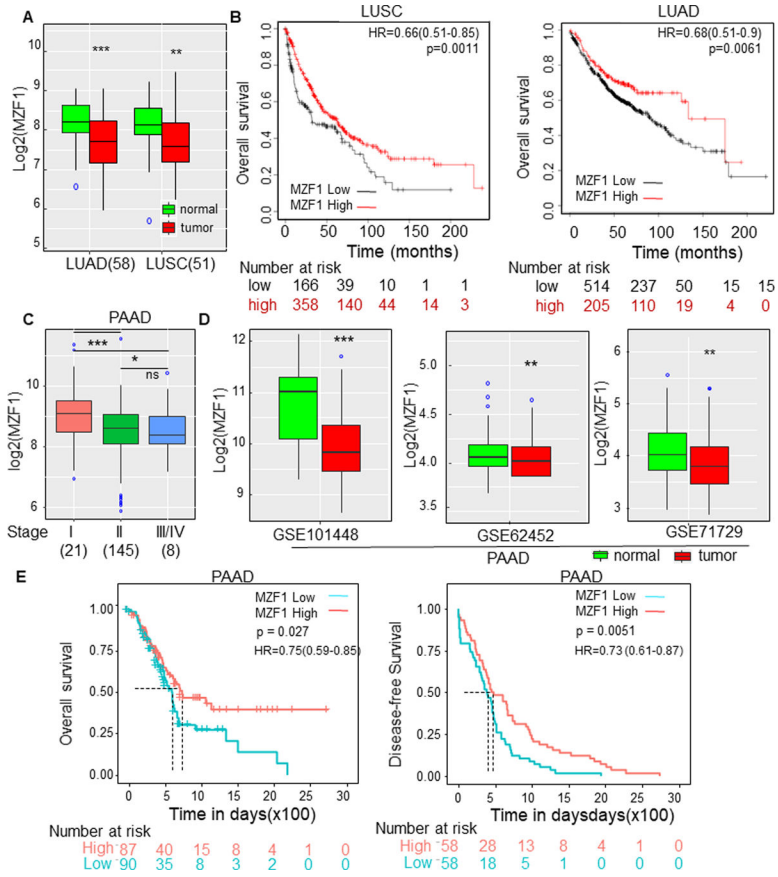

Fig. 7. Reduced MZF1 expression in tumors correlates with poor patient survival in NSCLC and PAAD.

(A) MZF1 expression is decreased in tumor tissues of LUAD and LUSC, the 2 major subtypes of NSCLC, as compared with paired non-tumor tissues.

(B) Reduced MZF1 expression correlates with poor overall survival in LUAD (left) and LUSC (right) patients based on Kaplan-Meier analysis of GEO data.

(C) MZF1 expression is reduced in tumors from stage II and II/IV PAAD patients as compared to those from stage I patients.

(A, C) Logarithmically (log_2) transformed MZF1 expression levels based on RNA sequencing data from PAAD patients in TCGA were compared by paired t-tests between tumor and normal tissues (A) or among tumors of different stages determined at diagnosis (C).

(D) MZF1 expression is decreased in tumors as compared to adjacent non-tumor tissues from PAAD patients, based on analysis of GEO datasets GSE101448 (left), GSE62452 (middle) and GSE71729 (right). Box plots represent quartile of normalized gene expression levels with relative intensity (log2) of microarray data from PAAD patients in these GEO datasets that compared between tumor and normal tissues.

(E) Reduced MZF1 expression correlates with poor overall survival (left) and disease-free survival (right) in PAAD patients based on Kaplan-Meier analysis of TCGA data.

(A, C-D) Horizontal lines represent median values. The bottom and top of the box are the first and third quartiles, with whiskers extending to 1.5 Interquartile range of the lower and

upper quartile respectively. The blue hollow circles represent outliers. ns, not significant, $p > 0.05$; *$p < 0.05$; **$p < 0.01$, ***$p < 0.001$ vs normal tissues (A, D) or for indicated comparisons (C) by Student's t test.

(B, E) p values from log-rank tests and Hazard ratio (HR) are indicated in the graphs

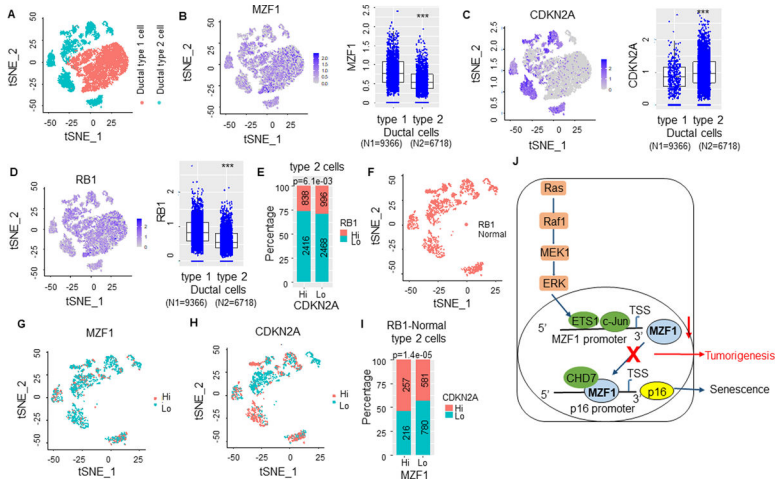

Fig. 8. Analysis of single cell RNA-seq data reveals a correlation between low MZF1 expression and reduced CDKN2A/p16^{INK4A} expression in PAAD.

(A) The t-distributed stochastic neighbor embedding (t-SNE) map of 16084 ductal cells grouped into ductal cell type 1 (normal cells) (orange) and ductal cell type 2 (tumor cells) (aqua blue).

(B-D) Expression levels of MZF1 (B), CDKN2A/p16^{INK4A} (C) and RB1 (D) are plotted onto the t-SNE map, showing decreased expression of MZF1 and RB1 and increased expression of p16^{INK4A} in the type 2 as compared to the type 1 ductal cells (left). MZF1 (B), CDKN2A/p16^{INK4A} (C) and RB1 (D) expression levels are directly compared between the type 1 and type 2 ductal cells in the box plots (right), with each dot representing expression level in each cell. The horizontal lines in the box are the median values, and the bottom and top of the box are the first and third quartiles. *** $p < 0.001$ vs type 2 by Student's t test.

(E) Percentage of type 2 ductal cells with high or low levels of CDKN2A/p16^{INK4A} that express high (orange) or low (aqua blue) levels of RB1. Type 2 ductal cells were divided into CDKN2A/p16^{INK4A}-high and -low groups using the median CDKN2A/p16^{INK4A} expression level as threshold; the number of cells with higher than/equal to or lower than median RB1 expression levels were counted in each group to determine the percentage of cells with high- or low-RB1 expression, respectively. The indicated p value was from Fisher's exact tests comparing the difference between the CDKN2A/p16^{INK4A}-high and -low groups. Number of single cells in each group is indicated in the columns.

(F) The t-SNE plot showing type 2 ductal (tumor) cells with normal RB1 expression levels, defined as those in which RB1 expression levels were higher than or equal to the median RB1 level in the type 1 normal ductal cells.

(G-H) The t-SNE plots of type 2 ductal cells with normal RB1 expression levels, showing cells with higher than/equal to the median (Hi, orange) or lower than the median (Lo, aqua blue) expression levels of MZF1 (G) or CDKN2A/p16^{INK4A} (H).

(I) Percentage of type 2 ductal cells with normal RB1 expression levels and high or low levels of MZF1 that express high (orange) or low (aqua blue) levels of CDKN2A/p16^{INK4A}. Type 2 ductal cells with normal RB1 expression levels (as shown in F) were divided into MZF1-high (Hi) and -low (Lo) groups using the median MZF1 expression level as threshold; the number of cells with higher than/equal to or lower than the median CDKN2A/p16^{INK4A} expression levels were counted in each group to determine the percentage of cells

with high (Hi) - or low (Lo)-CDKN2A/p16^{INK4A} expression, respectively. The indicated p value was from Fisher's exact tests comparing the difference between the MZF1-high and -low groups. Number of single cells in each group is indicated in the columns.

(J) A proposed signaling pathway underlying the role of MZF1 in oncogenic *ras*-induced senescence. Upon activation of the Raf-MEK1-ERK cascade by oncogenic *ras*, ERK activates ETS1 and c-Jun through phosphorylation, which bind to the MZF1 promoter and induce MZF1 transcription. MZF1 in turn binds to the CDKN2A/p16^{INK4A} promoter and recruits CHD7, which stimulates CDKN2A/p16^{INK4A} transcription, leading to induction of senescence. It is likely that in NSCLC and PAAD cells with normal RB1 expression, decreased MZF1 expression contributes to reduction in p16^{INK4A} expression, disruption of senescence and enhanced tumorigenesis. Events that occur in cancer cells are indicated in red.